JOURNAL OF COMPUTATIONAL PHYSICS **130,** 191–202 (1997)
ARTICLE NO. CP965577

Explicit Time Marching Methods for the Time-Dependent Euler Computations

C. H. Tai,* D. C. Chiang,† and Y. P. Su†

*Department of Mechanical Engineering; †Department of System Engineering, Chung Cheng Institute of Technology, Taoyuan, Taiwan 33509, Republic of China

Received December 28, 1995; revised August 20, 1996

Four explicit type time marching methods, including one proposed by the authors, are examined. The TVD conditions of this method are analyzed with the linear conservation law as the model equation. Performance of these methods when applied to the Euler equations are numerically tested. Seven examples are tested, the main concern is the performance of the methods when discontinuities with different strengths are encountered. When the discontinuity is getting stronger, spurious oscillation shows up for three existing methods, while the method proposed by the authors always gives the results with satisfaction. The effect of the limiter is also investigated. To put these methods in the same basis for the comparison the same spatial discretization is used. Roe's solver is used to evaluate the fluxes at the cell interface; spatially second-order accuracy is achieved by the MUSCL reconstruction.

1. INTRODUCTION

For computation of the inviscid compressible flows the Euler equations are generally represented in the conservation law form as a hyperbolic system. Lacking the mathematic tool to analyze this nonlinear system, the linear scalar conservation law is frequently used as the model equation for theoretical analysis of the numerical methods. The methods can then be applied to the Euler equations and justified by the numerical experiments. However, there is still some difference between the theoretical analysis and real application to the Euler equations, especially when strong discontinuity is involved in the solution.

The numerical methods used in solving the hyperbolic system can be divided into the spatial and the temporal discretization. In the past few decades, numerous remarkable works have been made to give the understanding and insight of the numerical procedures, e.g., [1–12]. But relatively few attention has been paid to the explicit time marching methods. This may due to that the application of the explicit time marching method is rather straightforward. Several currently used methods such as the Euler forward method, the predictor–corrector method, and the Runge–Kutta method are regarded as well developed. Since they are simple and, in general, accurate enough, these methods are very good candidates for the computations of the time-dependent compressible flows. Although these methods succeed in different cases, detailed comparison is still lacking and the choice among these methods is rather a matter of taste. In this paper, four kinds of the explicit time marching methods are compared with the same spatial discretization implemented. The four methods tested are the Euler forward method, the predictor–corrector method, the Runge–Kutta method, and one proposed by the authors.

As is well known nowadays, with high order of accuracy, linear schemes will generate spurious oscillation wherever the solution is not smooth. Recently, the concept of TVD [7] has been widely adopted to prevent the spurious oscillation. The methods studied in this paper are thus derived in their TVD form. The linear scalar conservation law is used to analyze the conditions for different methods to be TVD. To put all methods in the same basis for the comparison, the fluxes at the cell interface are evaluated with Roe's solver [5], the MUSCL approach [4] is adopted to get second-order accuracy in space.

Originated by Van Leer [3] and also by Boris and Book [2], a nonlinear function, called a limiter, should be used to make a second-order scheme TVD. The choice of the limiter function is, in general, problem dependent. In many circumstances the choice of the limiter is no more than a rule of thumb. In this paper, the performance of different methods with different limiters are also examined.

This paper is composed of five sections. The formulation of all methods examined are given in Section 2. Using the linear scalar conservation law, the methods are theoretically analyzed in Section 3. In Section 4, the methods are numerically tested with different examples. The conclusions are given in the Section 5.

2. NUMERICAL PROCEDURE

In the conservation law form, the Euler equations can be expressed as

$$U_t + F(U)_x = 0, \tag{1}$$

0021-9991/97 $25.00

where $U = [\rho, \rho u, \rho E]^T$, $F(U) = [\rho u, \rho u^2 + p, \rho u H]^T$ and for the ideal gas the constitute equation $p = (\gamma - 1)\rho(E - u^2/2)$. To solve Eq. (1), the spatial derivative term is first discretized and then the solution is advanced by different time marching methods as described below.

2.1. *The Spatial Discretization*

Since there are four kinds of time marching methods examined here. To make the results comparable to each other, the spatial discretization is kept the same as possible. For all methods, the fluxes at the cell interfaces are evaluated with Roe's solver [5] as

$$F_I = \frac{1}{2}(F^L + F^R) - \frac{1}{2}\sum_{k=1}^{3} |\hat{a}_k| \hat{R}_k \Delta V_k. \tag{2}$$

The matrix $\hat{R}$ is composed of the right eigenvectors of the Jacobian matrix. For the ideal gas it reads

$$\hat{R} = \begin{bmatrix} 1 & 1 & 1 \\ \hat{u} - \hat{c} & \hat{u} & \hat{u} + \hat{c} \\ \hat{H} - \hat{u}\hat{c} & \frac{1}{2}\hat{u}^2 & \hat{H} + \hat{u}\hat{c} \end{bmatrix}, \tag{3}$$

and the vector ΔV is defined as

$$\Delta V = \frac{1}{\hat{c}^2} \begin{bmatrix} \frac{1}{2}(\Delta p - \hat{\rho}\hat{c}\Delta u) \\ \hat{c}^2 \Delta\hat{\rho} - \Delta p \\ \frac{1}{2}(\Delta p + \hat{\rho}\hat{c}\,\Delta u) \end{bmatrix}. \tag{4}$$

The eigenvalues $\hat{a}_k$ are the characteristic speeds $\hat{u} - \hat{c}$, $\hat{u}$ and $\hat{u} + \hat{c}$, where the modification due to van Leer *et al.* [13] is made to exclude the unphysical expansion shock. The modification is

$$|\hat{a}_k|^* = \begin{cases} |\hat{a}_k|, & |\hat{a}_k| \geq \frac{1}{2}\delta a_k \\ \dfrac{\hat{a}_k^2}{\Delta a_k} + \dfrac{1}{4}\delta a_k, & |\hat{a}_k| \leq \frac{1}{2}\delta a_k, \end{cases} \tag{5}$$

where $\Delta a_k = a_k^{\mathrm{R}} - a_k^{\mathrm{L}}$ and $\delta a_k = 4\ \max(\Delta a_k, 0)$. The subscript k represents the kth eigenvalue and the superscripts R and L stand for the *right* and *left* sides of the interface. In Eq. (5) no free parameter needs to be tuned; the same modification is made to all the computations in this paper. Hereafter, the superscript * will be dropped, the modification will be considered as a part of Roe's solver and will not be explicitly mentioned. In Eqs. (3), (4), and (5) the variables with a hat are the Roe-averaged values; those without a hat are the cell-averaged values.

To bring the spatial accuracy up to second order, the MUSCL approach is adopted. The interface values are reconstructed as

$$\begin{aligned} W_{i+1/2} &= W_i + \tfrac{1}{2}\delta W_i \\ W_{i-1/2} &= W_i - \tfrac{1}{2}\delta W_i, \end{aligned} \tag{6}$$

where δW is the gradient of the state variables and evaluated with the appropriate limiter. Two limiters are examined in this paper and read

$$\delta\phi_j = \mathrm{ave}(\theta_j - \phi_{j-1}, \phi_{j+1} - \phi_j),$$

$$\mathrm{ave}(a, b) = \begin{cases} \min \mathrm{mod}(a, b), & ab > 0 \\ 0, & ab \leq 0, \end{cases} \tag{7a}$$

$$\mathrm{ave}(a, b) = \begin{cases} \min \mathrm{mod}\{\max \mathrm{mod}(a, b), \min \mathrm{mod}(2a, ab)\}, & ab > 0 \\ 0, & ab \leq 0. \end{cases} \tag{7b}$$

In the following, we call Eq. (7a) the *minmod* limiter and Eq. (7b) the *superbee* limiter [14]. By limiting the gradients, the limiter adds a certain amount of dissipation to the scheme. The *minmod* is the most dissipative and the *superbee* is the least dissipative. The difference between these limiters will be tested and discussed in Section 4. For consistency in all methods described below, the limiter is applied to the primitive variables, i.e., ρ, u, p.

2.2. *The Time Integration Methods*

Four methods are tested in this paper, the discretized formulations are given below. The Euler method (denoted as the E method hereafter) can be written as

$$U_i^{n+1} = U_i^n - \lambda(F_{i+1/2}^n - F_{i-1/2}^n), \tag{8}$$

where λ is the mesh ratio,

$$\lambda = \Delta t/\Delta x. \tag{9}$$

For simplicity, we use the U_i^n and F_i^n to represent the numerical evaluations of U and F at position $i\Delta x$ and time $n\Delta t$. To shorten the notation, the time or spatial indices may be dropped whenever there is no ambiguity.

Equation (8) is a spatially second-order scheme and temporally a first-order scheme. The linear version of this

scheme is linearly unconditionally unstable. However, as will be shown in the next section, with the TVD constraint imposed the nonlinear version of this scheme is conditionally stable.

The second method considered is the Hancock method [15] (denoted as the H method hereafter) and given as

$$U^{n+1} = U^n - \lambda(\tilde{F}_{i+1/2} - \tilde{F}_{i-1/2}). \tag{10}$$

Where $\tilde{F} = F(\tilde{U})$ and $\tilde{U}$ is evaluated by the predictor step. For the predictor step, the primitive variables are used instead of the conservative variables. Denote the primitive variables as

$$W = [\rho \quad u \quad p]^{\mathrm{T}}, \tag{11}$$

the predictor step is

$$\tilde{W}_i = W_i - \frac{\Delta t}{2\Delta x} A_W \delta W_i \tag{12}$$

and the Jacobian matrix reads

$$A_W = \begin{bmatrix} u & \rho & 0 \\ 0 & u & \dfrac{1}{\rho} \\ 0 & \rho c^2 & u \end{bmatrix}. \tag{13}$$

Note that, the gradient only needs be evaluated once, the same value is used for both the predictor and corrector steps. This will not affect the second-order accuracy, as will be shown in the next section. The predictor step is much cheaper than the corrector step in computational cost.

Different types of the Runge–Kutta (RK) methods have been successfully incorporated to solve the hyperbolic system for steady or unsteady problems, e.g., [16, 17]. Here, a two-stage second-order method is considered and written as

$$\begin{aligned} U^{(0)} &= U^n \\ U^{(1)} &= U^{(0)} - \tfrac{1}{2}\lambda(F^{(0)}_{i+1/2} - F^{(0)}_{i-1/2}) \\ U^{(2)} &= U^{(0)} - \lambda(F^{(1)}_{i+1/2} - F^{(1)}_{i-1/2}) \\ U^{n+1} &= U^{(2)} \end{aligned} \tag{14a}$$

where $F^{(0)} = F(U^{(0)})$ and $F^{(1)} = F(U^{(1)})$.

The last method examined here is the one modified by the authors, which is the combination of the above two methods. In the RK method an H method is used to get the state variables at each stage:

$$\begin{aligned} U^{(0)} &= U^n \\ U^{(1)} &= U^{(0)} - \tfrac{1}{2}\lambda(\tilde{F}^{(0)}_{i+1/2} - \tilde{F}^{(0)}_{i-1/2}) \\ U^{(2)} &= U^{(0)} - \lambda(\tilde{F}^{(1)}_{i+1/2} - \tilde{F}^{(1)}_{i-1/2}) \\ U^{n+1} &= U^{(2)}. \end{aligned} \tag{14b}$$

Again, the ˜ means the predictor step is incorporated. However, in Eq. (14b) only half of a time step is forwarded for each stage, so Eq. (12) becomes

$$\tilde{W}_i = W_i - \frac{\Delta t}{4\Delta x} A_W \delta W_i. \tag{15}$$

3. THE LINEAR SCALAR CONSERVATION LAW

Before presenting the numerical results some theoretical analysis is made here. Since the mathematic tool for the analysis of nonlinear systems is still lacking, the linear conservation law is used as the model equation. The equation is

$$\frac{\partial u}{\partial t} + \frac{\partial f}{\partial x} = 0, \tag{16}$$

where $f = au$, a is a constant, and only $a > 0$ is considered in the following. The analysis for the case $a < 0$ follows the same way.

Rewrite the E method, Eq. (8), for this case as

$$u_i^{n+1} = u_i^n - \lambda(f^n_{i+1/2} - f^n_{i-1/2}). \tag{17}$$

By Eq. (2) and (6) the numerical flux is now reduced to

$$f_{i+1/2} = a(u_i + \tfrac{1}{2}\delta u_i) \tag{18a}$$

and

$$f_{i-1/2} = a(u_{i-1} + \tfrac{1}{2}\delta u_{i-1}). \tag{18b}$$

As mentioned above, the gradient should be *limited.* For the following analysis, Eq. (7) is now reformulated as

$$\begin{aligned} \delta\phi_i &= \mathrm{ave}(\phi_i - \phi_{i-1}, \phi_{i+1} - \phi_i) \\ &= (\phi_i - \phi_{i-1})\varphi(r_i), \end{aligned} \tag{19}$$

where

$$r_i = \frac{\phi_{i+1} - \phi_i}{\phi_i - \phi_{i-1}}.$$

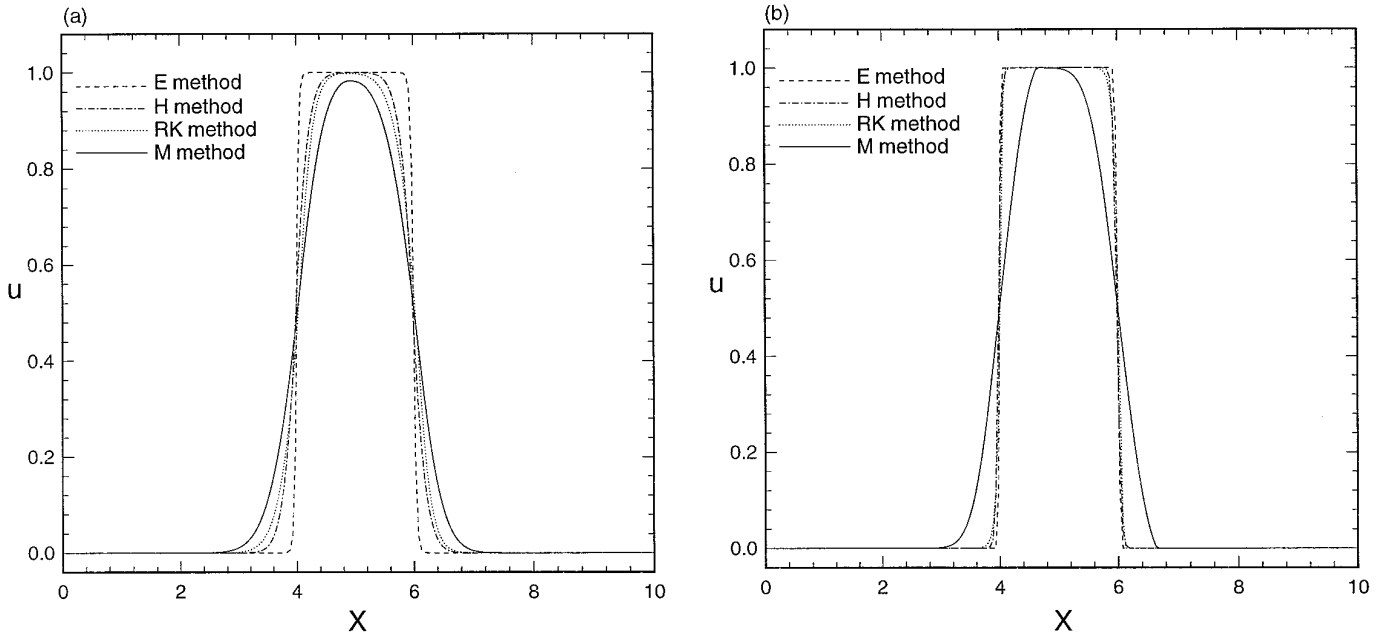

FIG. 1. Solutions of Example 1: (a) with *minmod* limiter; (b) with *superbee* limiter. $\nu = 0.5$ and $\Delta x = 0.05$.

Using the notation $\Delta_{i-1/2}\phi = \phi_i - \phi_{i-1}$ and $\varphi_i = \varphi(r_i)$, Eq. (19) becomes

$$\delta\phi_i = \varphi_i \Delta_{i-1/2}\phi. \tag{20a}$$

Similarly we can have

$$\delta\phi_{i-1} = \frac{\varphi_{i-1}}{r_{i-1}} \Delta_{i-1/2}\phi. \tag{20b}$$

So, Eq. (7) becomes

$$\varphi(r) = \begin{cases} \min \text{mod}(1, r), & r > 0, \\ 0, & r \le 0; \end{cases} \tag{21a}$$

$$\varphi(r) = \begin{cases} \min \text{mod}[\max \text{mod}(1, r), \min \text{mod}(2, r)], & r > 0, \\ 0, & r \le 0. \end{cases} \tag{21b}$$

One may note that, in real computations Eq. (7) is used instead of Eq. (21). Since Eq. (21) is not defined when $\phi_i - \phi_{i-1} = 0$; this difficulty will not happen with Eq. (7).

Put Eq. (18) and (20) into Eq. (17); the fully discretized equation reads

$$u^{n+1} = u^n - \nu \left[1 + \frac{1}{2} \left(\varphi_i - \frac{\varphi_{i-1}}{r_{i-1}} \right) \right] \Delta_{i-1/2} u, \tag{22}$$

where ν is the Courant number and is defined as

$$\nu = a \frac{\Delta t}{\Delta x}.$$

To shorten the formulas, define

$$\Psi = \varphi_i - \frac{\varphi_{i-1}}{r_{i-1}}. \tag{23}$$

Harten [18] has been able to show that for Eq.(22) to be TVD the sufficient conditions are

$$1 \ge \nu(1 + \tfrac{1}{2}\Psi) \ge 0. \tag{24}$$

Require the Ψ to be bounded as $|\Psi| \le \alpha$, the inequality (24) can be cast into

$$1 \ge \nu(1 + \tfrac{1}{2}\alpha) \tag{25a}$$

and

$$\nu(1 - \tfrac{1}{2}\alpha) \ge 0. \tag{25b}$$

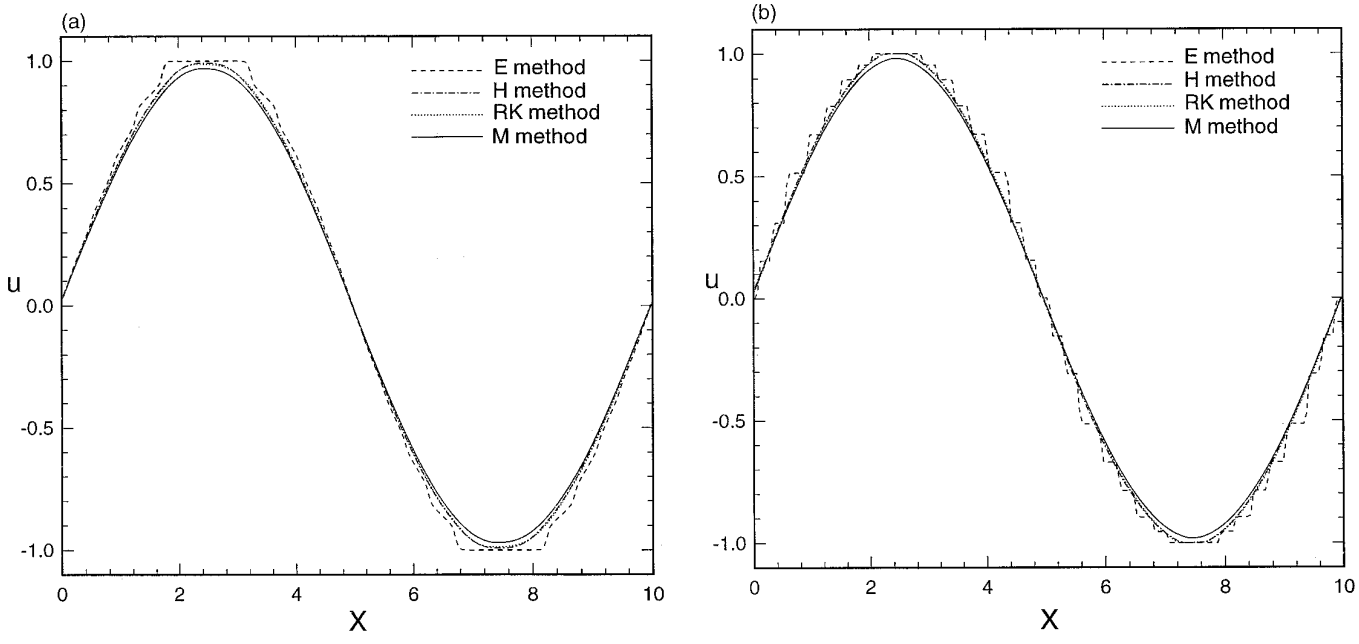

FIG. 2. Solutions of Example 2: (a) with *minmod* limiter; (b) with *superbee* limiter. $\nu = 0.5$ and $\Delta x = 0.05$.

The sufficient conditions for Eq. (22) to be TVD thus become

$$\alpha \le 2 \tag{26a}$$

and

$$\nu \le \frac{2}{2+\alpha}. \tag{26b}$$

Similarly, the discretized equations for other methods are

$$u^{n+1} = u^n - \nu\left(1 + \frac{1-\nu}{2}\Psi\right)\Delta_{i-1/2}u \tag{27}$$

$$u^{n+1} = u^n - \nu\left(1 + \frac{\Psi}{2}\right)\left[1 - \frac{\nu}{2}\left(1 + \frac{\Psi}{2}\right)\right]\Delta_{i-1/2}u - \frac{\nu^2}{2}\left(1 + \frac{\Psi}{2}\right)^2\Delta_{i-2/3}u \tag{28}$$

$$u^{n+1} = u^n - \nu\left(1 + \frac{2-\nu}{4}\Psi\right)\left[1 - \frac{\nu}{2}\left(1 + \frac{2-\nu}{4}\Psi\right)\right]\Delta_{i+1/2}u - \frac{\nu^2}{2}\left(1 + \frac{2-\nu}{4}\Psi\right)^2\Delta_{i-2/3}u, \tag{29}$$

where Eqs. (27), (28), and (29) correspond to the H, RK, and M methods, respectively. The CFL-like condition for different methods can be found as

$$\nu \le 1 \tag{30a}$$

$$\nu \le \frac{2}{2+\alpha} \tag{30b}$$

$$\nu \le \frac{\alpha + 2 - \sqrt{\alpha^2+4}}{\alpha}, \tag{30c}$$

where conditions (30a), (30b), and (30c) are subject to the methods H, RK, and M, respectively. Equation (26a) also must hold simultaneously with Eqs. (30). The bound of Ψ can be found for different limiters; for Eq. (21a), $\alpha = 1$ and for (21b), $\alpha = 2$. Due to Eq. (26a) it is clear that the *superbee* limiter is the upper bound for the methods to be TVD, where the lower bound is required by the second-order accuracy (see [8]). Also note that, Eqs. (28) and (29) contain the nonlinear combination of the ν and Ψ; Eqs. (30b) and (30c) only give the most restrictive conditions. In real computations we have found that with the Courant number larger than the ones restricted by Eq. (30b) or (30c) the methods can still be stable. But for the E and H methods, conditions (26b) and (30a), together with (26a), must be satisfied.

Using the linear average for the gradient in Eq. (18), that is

$$\delta u_i = \frac{u_{i+1} - u_{i-1}}{2}. \tag{31}$$

The unlimited (linear) form of the above methods can be achieved. The procedure is, although tedious, straightfor-

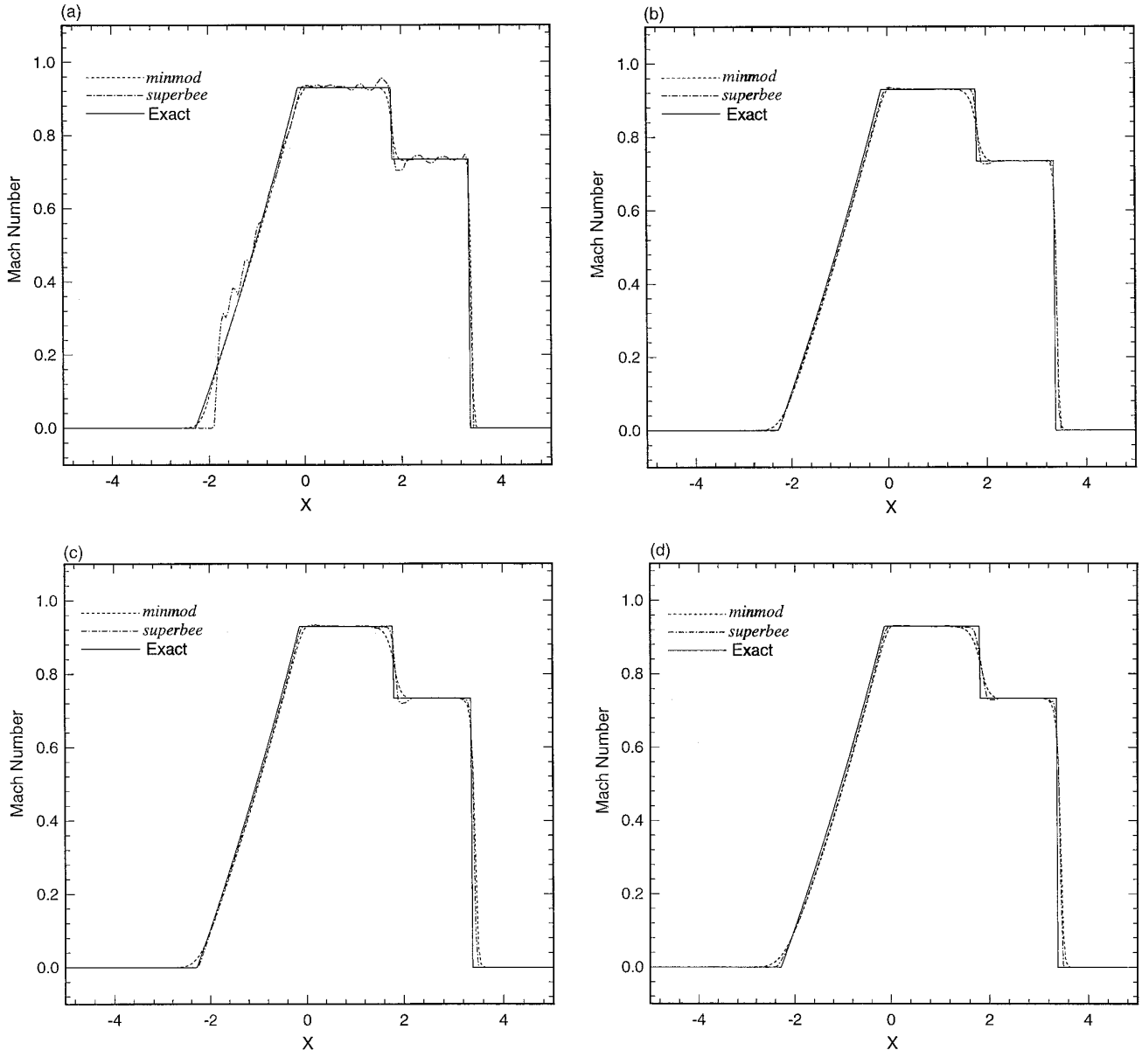

FIG. 3. Solutions of Example 3 at $t = 6.1 \times 10^{-3}$: (a) E method; (b) H method; (c) RK method; (d) M method. $\nu = 0.5$ and $\Delta x = 0.05$.

ward. Inserting the Taylor series expansion into the full discretized equations, which are now linear, the truncation errors of all methods can be easily found. The H and RK methods are second-order accurate. The lowest order truncation error of the E method is $-\nu a \Delta x u_{xx}/2$, while it is $\nu a \Delta x u_{xx}/4$ for the M method. As mentioned in the previous section, in its linear version the E method is unconditionally unstable.

Surprisingly, the M method, being the most complicated one considered here, is only first-order accurate. However, this extra dissipation term could be helpful in eliminating the spurious oscillation, as will be shown in the next section.

4. NUMERICAL TEST

EXAMPLE 1. The methods are first tested against the Eq. (16). Set $a = 1$, $\Delta x = 0.05$, and give the initial condition as

$$\begin{aligned} u(x,0) &= 0, \quad 0 \le x < 4 \\ u(x,0) &= 1, \quad 4 \le x \le 6 \\ u(x,0) &= 0, \quad 6 < x \le 10. \end{aligned} \tag{31}$$

The periodic boundary condition is imposed at the both ends; Fig. 1 shows the results after the wave has turned a

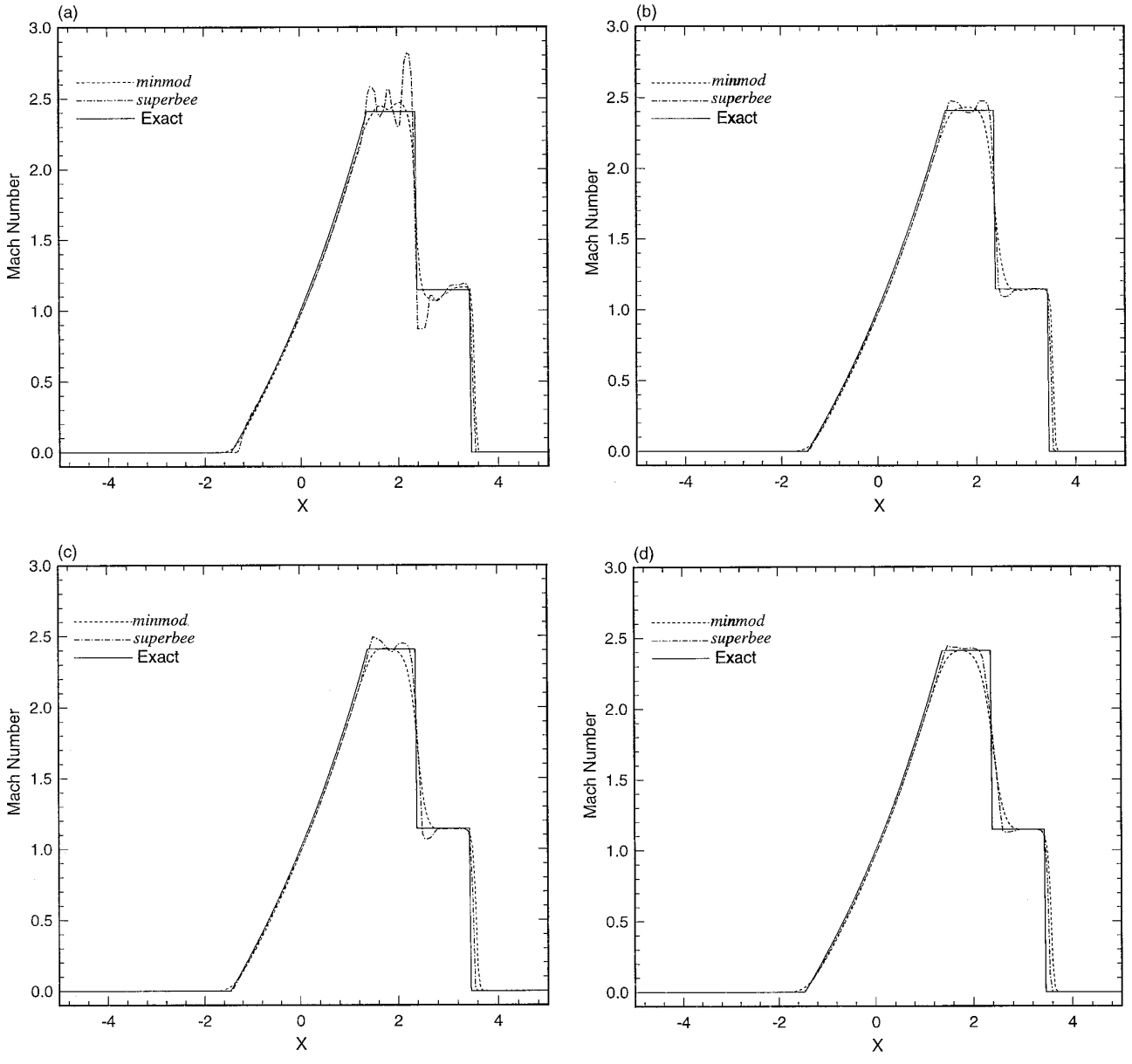

FIG. 4. Solutions of Example 4 at $t = 3.9 \times 10^{-3}$: (a) E method; (b) H method; (c) RK method; (d) M method. $\nu = 0.5$ and $\Delta x = 0.05$.

full cycle. The Courant number is chosen so that all methods are TVD. In Fig. 1a the *minmod* limiter is used, while in Fig. 1b the *superbee* limiter is used. According to Sweby [8], these two limiters are the upper and lower bounds of the second-order TVD schemes; other limiters perform somehow in between. It can be clearly seen in Fig. 1 that the M method is too dissipative compared with the other methods. Interestingly, the best results are given by the E method, which is only first order in time and takes the least computational effort.

EXAMPLE 2. Use the setting as in the previous example, Fig. 2 gives the results with the initial condition

$$u(x, 0) = \sin\left(\frac{\pi}{5}x\right), \quad 0 \le x \le 10. \tag{32}$$

Again, the *minmod* and *superbee* limiter is incorporated in Figs. 2a and 2b, respectively. One may note that, the stair-like solution of the E method does not mean it is not TVD. Besides the analysis in the previous section, the total variation is actually summed in the computations and it is not increasing. The computation has been continued to let the wave turn more cycles; the local extremas are well bounded. Since the stair-like solution is not acceptable, one way to cure this is by using a much smaller Courant

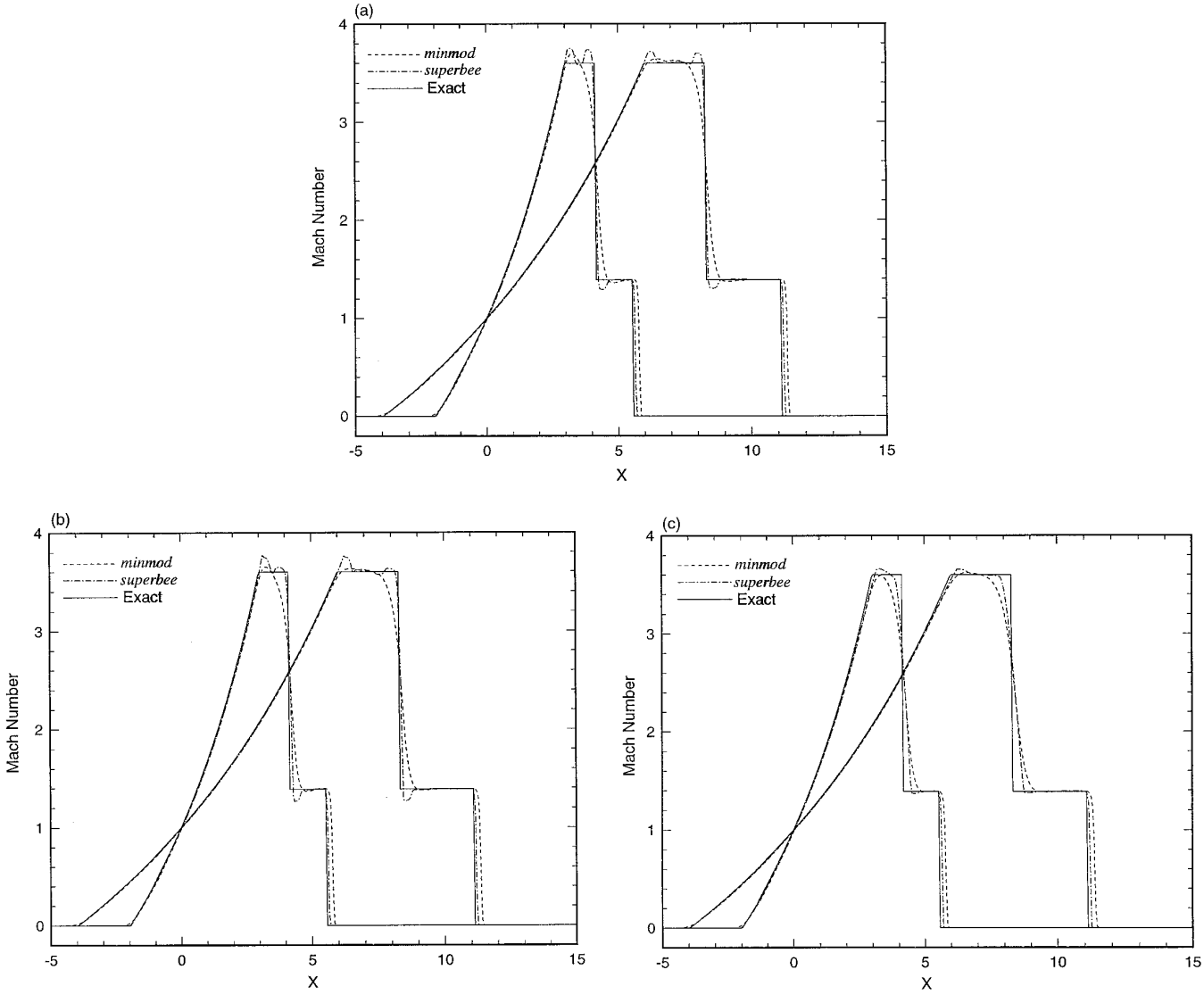

FIG. 5. Solutions of Example 5 at $t = 1.2$ and $t = 2.4$: (a) H method; (b) RK method; (c) M method. $\nu = 0.5$ and $\Delta x = 0.05$.

number. Thus, the attractiveness of the E method is lost. As pointed out in [8] the *superbee* limiter will turn a sine wave into a square wave. This is also observed in our work for the E, H, and RK methods. However, since the M method is more dissipative near a local extremum, the wave form is kept even with the *superbee* limiter.

From the above tests, we conclude that the M method is more dissipative near the local extrema; the extrema need not be discontinuities. The H and RK methods are approximately equivalent to each other, with the RK method being more computationally expensive than the H method. Considering the effects of different limiters, the *minmod* limiter always give more diffusive results for all methods, while the results of the M method with the *superbee* limiter are approximately equivalent to the results of the H or RK method with the *minmod* limiter.

Now we turn our attention to the Euler equations, i.e., Eq. (1). For the 1D inviscid compressible flows, the exact solution exists for the Reimann problem. So the numerical results can be tested without ambiguity.

EXAMPLE 3. The first case tested is Sod's problem with the initial conditions

$$\rho = 1, \quad u = 0, \quad p = 1 \times 10^5, \quad x \le 0,$$
$$\rho = 0.125, \quad u = 0, \quad p = 1 \times 10^4, \quad x > 0;$$

$\Delta x = 0.05$ and $\nu = 0.5$ are used for this and the next three cases. In this case the discontinuity is rather weak; the

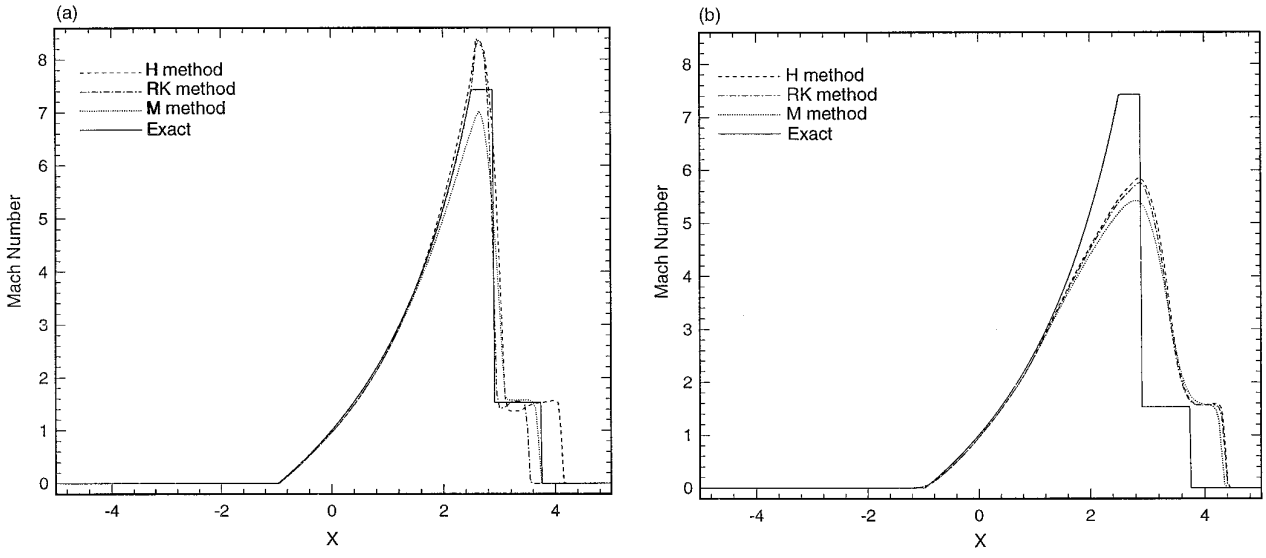

FIG. 6. Solutions of Example 6 at $t = 2.6 \times 10^{-3}$: (a) with *superbee* limiter; (b) with *minmod* limiter. $\nu = 0.5$ and $\Delta x = 0.05$.

results are shown in Fig. 3. In Fig. 3a, the results of the E method with the *superbee* limiter show the evident oscillation, while much better results are achieved with the *minmod* limiter. For the E method with the *superbee* limiter, reducing the Courant number cannot eliminate the oscillation effectively. Although not shown here, with $\nu = 0.25$ the results are still oscillatory.

The CPU time is also recorded for different methods. Take the CPU time for the E method as 1 unit. For each time step, the H method takes 1.0675 units, the RK method takes 1.9656 units, and the M method takes 2.143 units.

EXAMPLE 4. For the second case we consider the stronger discontinuity with the initial conditions

$$\rho = 1, \quad u = 0, \quad p = 1 \times 10^5, \quad x \le 0,$$
$$\rho = 1 \times 10^{-2}, \quad u = 0, \quad p = 1 \times 10^3, \quad x > 0.$$

Figure 4 shows the results of different methods with two limiters. Again, the E method cannot give satisfactory results. Resolution of the shock is about the same for all methods, while for the M method the contact discontinuity is slightly more diffusive than those by other methods. When using the *superbee* limiter there are over- and undershoots near the contact discontinuity for all methods. However, these shoots are scarcely noticeable for the M method.

EXAMPLE 5. This case is used by Kim and Liu [19] and called the *"strong shock problem"* by them. Using the same values as in [19], the initial conditions are

$$\rho = 400, \quad u = 0, \quad p = 500, \quad x \le 0,$$
$$\rho = 1, \quad u = 0, \quad p = 1, \quad x > 0.$$

Figure 5 presents the results by different methods at $t = 1.2$ and $t = 2.4$. The results of the E method are no longer shown, since they are not comparable with the results of other methods. The over- and undershoots are now more evident for the H and RK methods with the *superbee* limiter, while the *minmod* limiter is effective in eliminating the oscillation. We have found from the numerical test that, with the *superbee* limiter, reducing the Courant number can only reduce the amplitude of the oscillation; it cannot eliminate it. A leading error of the shock position can also be observed in Fig. 5. However, this error does not change with respect to time, so the wave speeds should be correct.

Note that until now the same limiter gives approximately the same shock profile for all methods. With different limiters the shock is only slightly deviated. In all cases tested above, the wave speeds are correctly predicted.

EXAMPLE 6. Consider the case with extremely strong discontinuity for the initial condition set as

$$\rho = 1, \quad u = 0, \quad p = 1 \times 10^5, \quad x \le 0,$$
$$\rho = 1 \times 10^{-4}, \quad u = 0, \quad p = 1 \times 10^1, \quad x > 0.$$

The results are shown in Fig. 6.

This is the only case in which we see a significant error of the shock position. With the *superbee* limiter the H method shows a leading error and the RK method shows

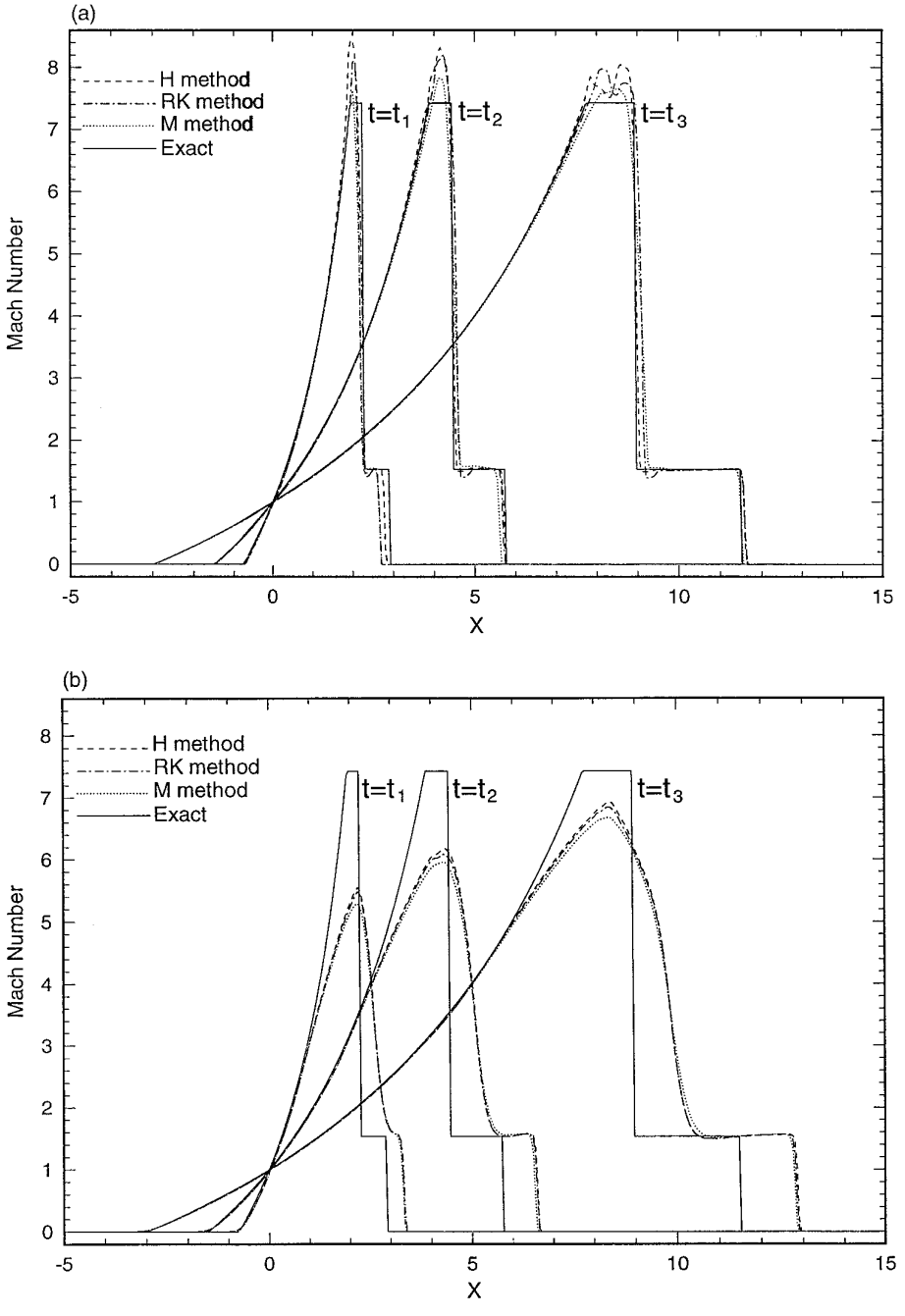

FIG. 7. Solutions of Example 6 at $t_1 = 2 \times 10^{-3}$, $t_2 = 4 \times 10^{-3}$, and $t_3 = 8 \times 10^{-3}$: (a) with *superbee* limiter; (b) with *minmod* limiter. $\nu = 0.25$ and $\Delta x = 0.05$.

a lagging error. When using the *minmod* limiter all methods get approximately the same leading error of the shock position, which is larger than the ones with the *superbee* limiter.

To further explore this problem, the case has been run for a longer time with a smaller Courant number $\nu = 0.25$. The results at different times are shown in Fig. 7. The error of the shock position is significantly reduced for all methods with the *superbee* limiter. However, with the *minmod* limiter, there are no improvements of the shock position. From Fig. 7b, one may note that the error of the shock position is linearly proportional to the time; this implies the shock speed is incorrectly predicted. In Fig. 7a there are lagging errors at the early times but they slowly approach the leading error for all methods.

Since we could not analyze the nonlinear system equa-

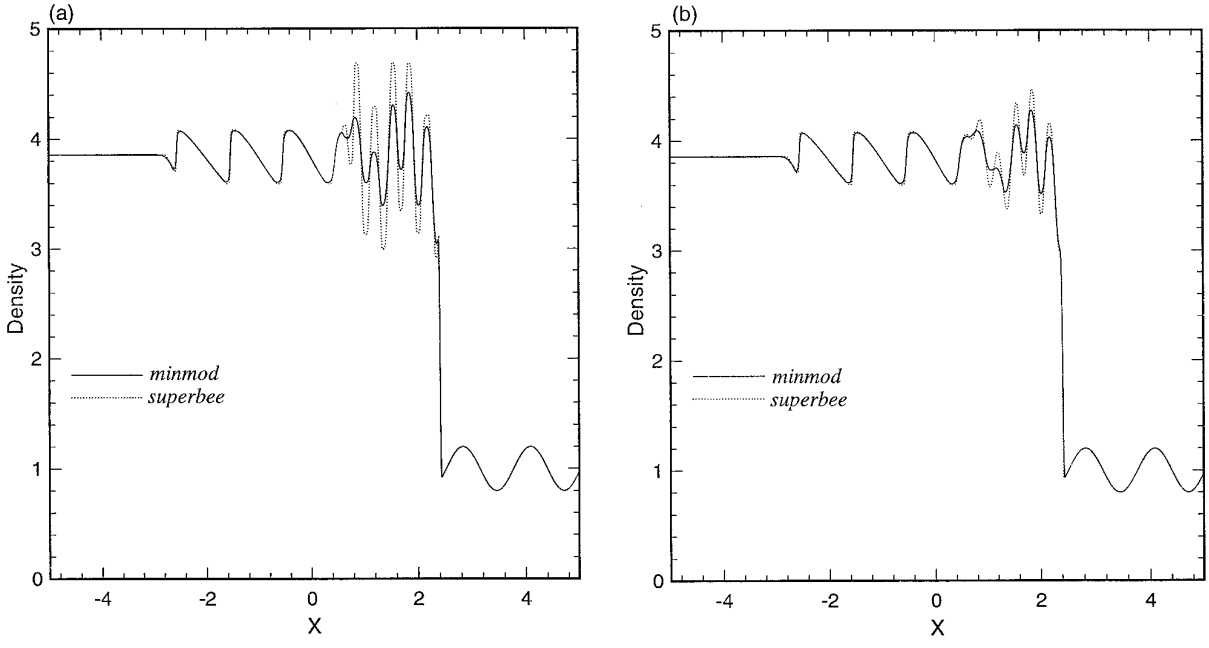

FIG. 8. Solutions of Example 7 at $t = 1.8$: (a) H method; (b) M method. $\nu = 0.5$ and $\Delta x = 0.0125$.

tions, the true reason of the error is not clear. For a linear scheme, the Von Nuemann analysis can be used to address the phase error. But the problem only shows up in this example; it must be associated with the extremely strong discontinuity, i.e., high nonlinearity. The Von Neumann analysis has been made for the linear versions of these methods; no conclusive results were obtained. The only recommendation we can make so far is to use the *superbee* limiter, together with a small Courant number when such strong discontinuity is encountered. Further investigation of this phenomenon is needed.

EXAMPLE 7. The above cases are rather *"simple"* in the flow patterns, a more *"complex"* case is tested here. This case is used by Shu and Osher [17] and the initial conditions are

$$\rho = 3.857143, \quad u = 2.629369, \quad p = 10.33333, \quad x < -4,$$
$$\rho = 1 + 0.2\sin 5x, \quad u = 0, \quad p = 1, \quad x \geq -4;$$

the results are shown in Fig. 8. For this case 800 cells are used. Since there are no exact solutions for this example, the readers may refer to [17], where third-order results are presented. As expected, the M method gives more diffusive results than the H method for the high frequency oscillation behind the shock. But for the rest the solutions are almost identical. However, the results for the M method with the *superbee* limiter are still incomparable with the results by the H method with the *minmod* limiter.

5. CONCLUSIONS

Four methods are examined and numerically tested in this paper. To compare these methods, not only the quality of the results but also the computational efficiency should be considered. The H method only takes about 7% more CPU time than the E method for each time step. This 7% CPU time can be easily compensated by using larger Courant numbers for the H method; compare Eq. (26b) with Eq. (30a). The H method performs much better than the E method. One may consider the H method better than the E method. The difference between the RK and M methods is quite similar to the difference between the E and H methods. Although the M method takes more CPU time than the RK method, larger Courant numbers can be used for the M method; compare Eqs. (30b) and (30c). The H and RK methods get similar results in most cases, but the RK method is much more time consuming than the H method. The choice is mainly between the H and M methods.

The H method is very good for a complex flow with weak discontinuity, as shown in Example 7. But when the discontinuity gets stronger, a more dissipative limiter is needed to eliminate the spurious oscillation. As mentioned before, the selection of the limiter is problem dependent. It is up to the user's knowledge to make the appropriate choice. In another way, one unique character of the M method is that it can stick with one limiter, the *superbee* limiter.

When extremely strong discontinuity is encountered the

best choice is the M method with the *superbee* limiter, as shown in Example 6. The shortcoming of the M method is that the contact discontinuity or the local extrema is diffusively resolved.

REFERENCES

1. S. K. Godunov, A difference scheme for the numerical computation of discontinuous solutions of hyperbolic equations, *Math. Sb.* **47,** 271 (1959); transl. U.S. Joint Publ. Res., JPRS 7726, 1969.
2. J. P. Boris and D. L. Book, Flux corrected transport. I. SHASTA, a fluid transport algorithm that works, *J. Comput. Phys.* **11,** 38 (1973).
3. B. van Leer, Towards the ultimate conservative difference scheme. I. The quest of monotinicity, in *Lecture Notes in Physics,* Vol. 18 (Springer Verlag, Berlin, 1973), p. 163.
4. B. van Leer, Towards the ultimate conservative difference scheme. V. A second order sequel to Godunov's method, *J. Comput. Phys.* **32** 101 (1979).
5. P. L. Roe, Approximate Reimann solvers, parameter vectors and difference schemes, *J. Comput. Phys.* **43,** 357 (1981).
6. B. Enquist and S. Osher, One-sided difference approximations for nonlinear conservation laws, *Math. Comput.* **36,** 321 (1981).
7. A. Harten, High resolution schemes for hyperbolic conservation laws, *J. Comput. Phys.* **49,** 357 (1983).
8. P. K. Sweby, High resolution schemes using flux limiters for hyperbolic conservation laws, *SIAM J. Numer. Anal.* **21,** 995 (1984).
9. P. Colella and P. Woodward, The piecewise parabolic method (PPM) for gas-dynamics simulations, *J. Comput. Physics* **54,** 174 (1984).
10. H. C. Yee, R. F. Warming, and A. Harten, Implicit total variation diminishing (TVD) schemes for steady-states calculations, *J. Comput. Phys.* **57,** 327 (1985).
11. C. W. Shu, Total-variation-diminishing time discretizations, *SIAM J. Sci. Stat. Comput.* 9, No. 6, Nov. (1988).
12. M. S. Liou and C. J. Steffen, A new flux splitting scheme, *J. Comput. Phys.* **107,** 23 (1993).
13. B. van Leer, W. T. Lee, and K. G. Powell, Sonic-point capturing, in *AIAA 9th Computational Fluid Dynamics Conference, June* 1989.
14. P. L. Roe, Some contributions to the modeling of discontinuous flows, in *Proc. 1983 AMS-SIAM Summer Seminar on Large Scale Computing in Fluid Mechanics,* Lectures in Applied Mathematics, Vol. 22 (SIAM, Philadelphia, 1983), p. 163.
15. G. D. van Albada, B. van Leer, and W. W. Roberts Jr., A comparative study of computational methods in cosmic gas dynamics, *Astron. Astrophys.* **108,** 76 (1982).
16. C. H. Tai, J. H. Sheu, and B. van Leer, Optimal multistage schemes for Euler equations with residual smoothing, *AIAA J.* **33,** No. 6 (1995).
17. C. W. Shu and S. Osher, Efficient implementation of essentially non-oscillatory shock-capturing schemes, II, *J. Comput. Phys.* **22,** No. 4/5, 517 (1993).
18. A Harten, ''On the Nonlinearity of Modern Shock-Capturing Schemes,'' ICASE Report 86-69, Oct. 1986.
19. H. D. Kim and N. S. Liu, A time-accurate high-resolution TVD scheme for solving the Navier–Stokes equation, *J. Comput. Fluids* **22,** No. 4/5, 517 (1993).